1-1-2012

Observation of field-induced polarization of valleys in p-type Sb 2Te 3 single crystals

Z J. Yue
University of Wollongong, zy709@uowmail.edu.au

C B. Zhu
University of Wollongong, cz210@uowmail.edu.au

S X. Dou
University of Wollongong, shi@uow.edu.au

Xiaolin Wang
University of Wollongong, xiaolin@uow.edu.au

Observation of field-induced polarization of valleys in p-type Sb_2Te_3 single crystals

Z. J. Yue, C. B. Zhu, S. X. Dou, and X. L. Wang*

Spintronic and Electronic Materials Group, Institute for Superconducting and Electronic Materials, AIIM Facility, Faculty of Engineering, University of Wollongong, North Wollongong, New South Wales 2500, Australia

(Received 29 May 2012; published 15 November 2012)

A flow of carriers along the c axis is extremely sensitive to the orientation of an in-plane magnetic field due to in-plane mass anisotropy in layered compounds. Based on this mechanism, a rotatable in-plane magnetic field has been applied as a valley valve to tune the contribution of each valley in p-type Sb_2Te_3 bulk single crystals to the total conductivity and interlayer magnetoresistance (MR). A valley-polarized current is generated, and the angular-dependent interlayer MR of up to 160% represents strong anisotropy. There are six inequivalent peaks over all temperature and magnetic field ranges. The giant MR results from the intravalley and intervalley hole Coulomb scattering in upper valence bands. The interlayer MR anisotropy originates from field-induced polarization of valleys, and Coulomb interaction-induced valley distortion. The strong anisotropy of the angular-dependent interlayer MR reflects strong anisotropies of carrier scattering time and effective mass in the six valleys and their inequivalent contributions to total magnetoconductivity and interlayer MR in p-type Sb_2Te_3 bulk.

DOI: 10.1103/PhysRevB.86.195120 PACS number(s): 72.20.My, 75.47.De

Antimony telluride (Sb_2Te_3) compounds have a rhombohedral phase with the space group R_{3m}-D^5_{3d} and consist of quintuple layers bonded by van der Waals forces.[1,2] p-type Sb_2Te_3 compounds are well known and have been intensively studied as excellent thermoelectric materials[3,4] which are widely used as thermoelectric energy converters, refrigerators, and thermostats operating near room temperature. The band structure features are significant for understanding and improving the physical properties of materials and their practical device applications. In the last few decades, electrical properties and band structure parameters have been investigated in Se- and Bi-doped Sb_2Te_3 through Hall effect, Shubnikov–de Haas effect (SdH), and thermoelectric effect.[5–8] Many-valley models were applied to estimate the parameters of electronic structures. This multivalley band structure plays a dominant role in the interlayer transport properties of Sb_2Te_3 crystals.[9] Recently, Sb_2Te_3 has drawn great attention again because it was identified as a three-dimensional (3D) topological insulator.[10,11] Topological insulators are a new class of materials that conduct electricity on their surface, but have a band gap inside, as a result of topologically protected surface states.[12,13] They have unique and fascinating electronic properties, such as quantum spin Hall effects and magnetoelectric effects, and have great potential applications in spintronics and quantum computation with higher energy efficiency.[14–16] The surface states in topological insulators have been mainly investigated by Angle-resolved photoemission spectroscopy (ARPES), scanning tunneling microscopy (STM), and theoretical calculations.[17] Bulk magnetotransport and electronic structure measurements are indispensable for further understanding of electronic band states and exploring potential practical application in magnetoelectronics for Sb_2Te_3. Up to now, the effects of multivalley electronic structure on the interlayer transport properties of Sb_2Te_3 and other multivalley semiconductors are still unknown.

In layered compounds, a flow of Dirac carriers along the interlayer is extremely sensitive to the orientation of an in-plane magnetic field due to in-plane mass anisotropy. The interlayer conductivity of carriers could be the sum of each valley's contribution in a multivalley system. A rotatable in-plane magnetic field can be applied as a valley valve to tune the contribution of each valley to the total conductivity and the magnetoresistance (MR). Field-induced polarization of Dirac valleys has been investigated in semimetallic bismuth (Bi) in a rotatable in-plane magnetic field.[18] A threefold symmetry of angular-dependent MR was observed in bismuth because of the huge in-plane mass anisotropy. Angular-dependent interlayer MR has also been successfully applied to map the two-dimensional (2D) Fermi surface (FS) and investigate in-plane anisotropy of layered metals and high-temperature superconductors.[19–23] Compared with ARPES measurements, which are sensitive to surface conditions, and Shubnikov–de Haas oscillations, angular-dependent interlayer MR measurements can provide bulk FS topology information at higher temperatures and lower fields directly. Motivated by these experimental observations, we have investigated angular-dependent interlayer MR in p-type Sb_2Te_3 single crystals and observed six inequivalent peaks corresponding to six field-induced polarized valleys. The observed six inequivalent peaks reflect strong anisotropy of carrier scattering time and effective mass in the six valleys and their inequivalent contributions to total interlayer conductivity.

The Sb_2Te_3 single crystals can easily be cleaved along the interlayer. The p-type Sb_2Te_3 sample $4 \times 4 \times 5$ mm^3 in size was cleaved from a 9% Bi-doped Sb_2Te_3 bulk crystal. The upper inset of Fig. 1 is a schematic view of the experiment configuration and the crystal axes. Four-probe measurements of interlayer magnetotransport between 2 and 300 K were conducted using a Quantum Design 14 T Physical Properties Measurement System (PPMS). A sample rotator was used to perform the measurements at different field orientations. The applied ac bias current was 5 mA, directed along the interlayer (C_3 axis). The resistance measurements were also along the interlayer with an in-plane magnetic field. Rotations of the sample in a constant field and temperature were used to measure the angular dependence of the interlayer MR. In the Hall effect measurements, a current $I = 500$ μA was applied for the same sample with different in-plane contacts. The field

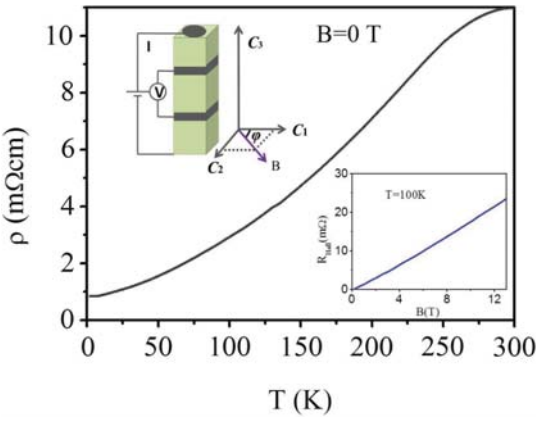

FIG. 1. (Color online) Temperature dependence of the zero-field resistance for the p-type Sb_2Te_3 single crystal. The upper inset displays a schematic view of experiment configuration and crystal axes and the lower inset shows the Hall resistance as a function of magnetic field at 100 K.

was increased from 0 to 13 T and was applied perpendicular to the plane. The temperature was fixed at 100 K, and detection of the voltage was perpendicular to both the current and the field direction.

Prior to the anisotropic interlayer MR measurements, the temperature dependence of the interlayer resistivity was measured. There are always significant differences between the in-plane and the interlayer resistivity because of anisotropy. Figure 1 shows the interlayer resistivity as a function of temperature for the p-type Sb_2Te_3 crystal, which represents a bulk metallic state. The interlayer resistivity decreases with decreasing temperature and approaches a constant value up to 8 K as shown in the lower inset of Fig. 1. The Hall effect measurement results demonstrate that the Hall resistance is positive and independent of temperature over the whole temperature range we measured. From the Hall measurements, we determined that the bulk average carrier density n is about 2×10^{19} cm^{-3}, and the bulk average carrier mobility μ is 1900 cm^2/V s, in agreement with what has been reported for typical p-type Sb_2Te_3 bulks.[5] Due to the high initial concentration of holes and the high Fermi energy in Sb_2Te_3, both valence bands were filled by holes. This is different from the carrier type in bismuth single crystals, in which electron pockets and hole pockets coexist in FS.

Figure 2(a) presents a series of measurements of the interlayer MR as a function of in-plane fields at different temperatures, ranging from 2 to 300 K, at 0°. The interlayer MR of the p-type Sb_2Te_3 crystal is proportional to the square of the magnetic field at low magnetic fields and shows linearity at high fields. The MR increases with decreasing temperature and reaches the maximum of 160% at 2 K ($\varphi = 0°$, $B = 13$ T). Figure 2(b) shows the interlayer MR with strong anisotropy at selected degrees. The MR reaches its maximum at $\varphi = 0°$ ($B = -13$ T) and 180° ($B = 13$ T). Very recently, we have observed room temperature giant and linear MR in a topological insulator Bi_2Te_3 nanosheet with a few quintuple layers.[24] The giant, linear MR achieved is as high as over 600% at room temperature without any sign of saturation at measured fields up to 13 T and was attributed to the quantum linear MR model developed by Abrikosov.[25] Due to high bulk hole concentration, the observed interlayer MR should result from bulk states rather than quantum linear MR from surface states in the p-type Sb_2Te_3. The charge carriers traveling along the interlayer are holes, and the interlayer MR is determined by the mobility of these carriers. The intravalley and intervalley scattering and Coulomb hole-hole interaction in the upper valence band result in the observed interlayer MR.[26] Impurity scattering might also play a role in the giant interlayer MR as well.

Figure 3(a) displays the angular-dependent interlayer MR for the Sb_2Te_3 at different temperatures: 2, 10, and 50 K in 13 T. On rotating the sample within the in-plane, the angular-dependent interlayer MR oscillation follows sixfold oscillations with two relative higher peaks at around 0° (360°) and 180°, and four relative lower peaks (crossed by dotted lines) at around 60° 120°, 240°, and 300° over the entire temperature range. With decreasing temperatures and increasing fields, the interlayer MR increases and the six peaks become more pronounced. This originates from the anisotropy of scattering time in six valleys, which is temperature dependent. Figure 3(b) presents the angular-dependent interlayer MR in different in-plane fields: 6, 9, and 13 T, at 2 K. The values of interlayer MR increase with

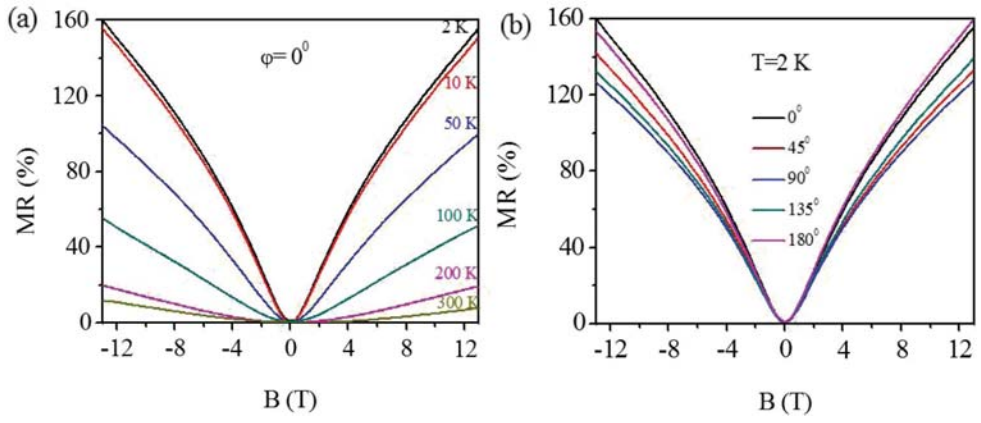

FIG. 2. (Color online) (a) Angular dependence of the interlayer MR as a function of field at different temperatures at $\varphi = 0^0$. (b) Angular dependence of interlayer MR as a function of field at different degrees at 2 K.

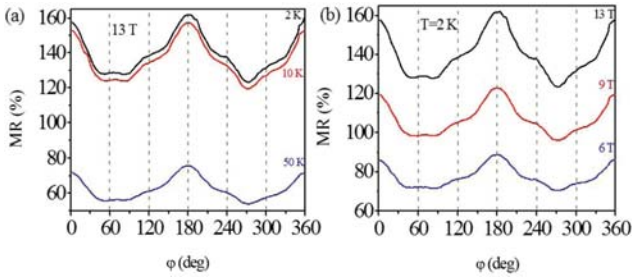

FIG. 3. (Color online) (a) Angular-dependent interlayer MR as a function of angular at different temperatures in 13 T in-plane magnetic fields. (b) Angular-dependent interlayer MR as a function of angular in different in-plane magnetic fields at 2 K.

increasing field, and the six peaks are most pronounced in high fields. The MR appears in the form of peaks when the in-plane magnetic field is oriented parallel or antiparallel to each valley. Actually, the sixfold oscillations are expected for the Sb_2Te_3 system with six valleys, while the strong anisotropy is beyond our prediction. Compared with sixfold symmetry observed in bismuth crystals, the six peaks in angular-dependent interlayer MR in Sb_2Te_3 are not symmetric and represent great differentiation. This differentiation might result from the differences of the carrier pockets and mass anisotropy in Bi and the *p*-type Sb_2Te_3. The temperature dependences of interlayer MR in Sb_2Te_3 are also different with the temperature and field dependence in Bi. The sixfold symmetry is spontaneously lost at lower temperatures and higher fields in Bi, which was attributed to a so-called nematic valley scenario and possible crystalline imperfections in the sample used.[18]

The ellipsoidal nonparabolic band model (Drabble-Wolf model) quite accurately describes the energy spectrum of the upper valence bands of Sb_2Te_3.[27] The FS of *p*-type Sb_2Te_3 always resides deep in the bulk valence bands. The valence band splits into two subbands with an energy difference: the upper valence bands (UVBs) and the lower valence bands (LVBs).[28] The UVB has six general ellipsoidal valleys, and each ellipsoid is centered on a mirror plane of the Brillouin zone. The six ellipsoidal valleys in both valence bands of Sb_2Te_3 are hexa-ellipsoidal and tilted with respect to the basal plane by a 45° angle.[29] The band gap E_g in Sb_2Te_3 is approximately 0.25 meV at room temperature and 0.26 meV at 4.2 K.[30] The energy gap ΔE between the UVB and LVB is about 30 meV for Sb_2Te_3.[5] Due to the high initial concentration of holes and the high Fermi energy in Sb_2Te_3, both valence bands were filled by holes. The hole carriers in the lower valence bands are heavy holes with lower mobility, while in the upper valence band, they are light holes with higher mobility. Both valence bands of Sb_2Te_3 consist of six ellipsoidal valleys tilted with respect to the basal plane, but the upper valence band is the one that mainly contributes to the bulk conductance. The anisotropies of effective mass ($m*$), scattering time (τ), and mobility (μ) in doped Sb_2Te_3 and Bi_2Te_3 were discovered through photoinduced transient thermoelectric effects.[5,31] The observed transient thermoelectric effects indicated a multirelaxation process for the carriers.

In the presence of effective mass anisotropy, anisotropic interlayer MR can be expected in an in-plane magnetic field. In this multivalley system, the interlayer conductivity represents the sum of the contributions from each valley in the energy bands in an in-plane magnetic field. The contributions from each of the six valleys can be modulated as the sample is rotated, and the interlayer MR can become an effective valley valve. In our case, the holes in the UVB of *p*-type Sb_2Te_3 dominate the total bulk conductivity. Figure 4 displays the schematic cross section of six valleys in the UVB of Sb_2Te_3 with and without in-plane magnetic field. The in-plane shape of field-polarized valleys in the Fermi surface has been reconstructed based on the angular-dependent interlayer MR in Sb_2Te_3. The valley degeneracy loses due to hole-hole Coulomb interaction and scattering in the presence of a strong in-plane magnetic field. The Coulomb interactions involve intervalley and intravalley scattering processes. With in-plane mass anisotropy, the Coulomb interaction energetically favors a spontaneous imbalance in the occupation of different valleys.[32–34] The angular dependence of interlayer MR is determined by the angular dependence of the cyclotron frequency, which is governed by the anisotropy of the cyclotron mass and the scattering time. The dominant contributions

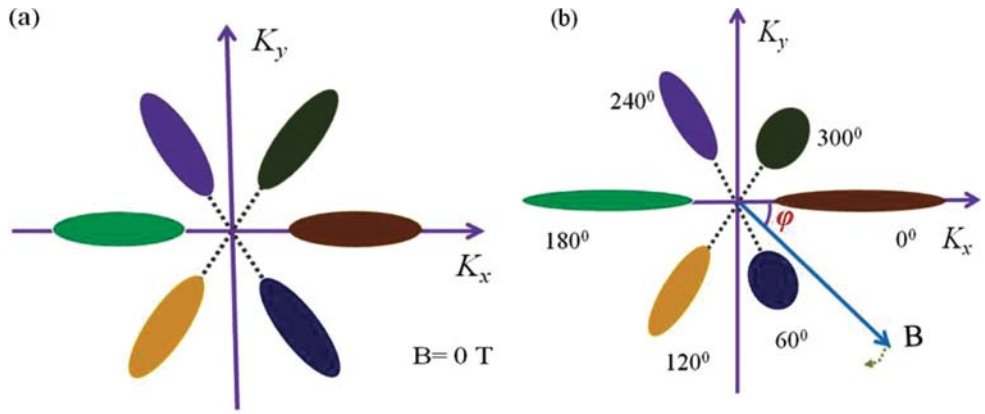

FIG. 4. (Color online) (a) A schematic cross-section view of valleys in K_x-K_y plane of the Brillouin zone without fields. (b) Schematic representation of polarized valley model fitted to the observed angular-dependent interlayer MR in a rotatable in-plane magnetic field. The interlayer conductivity is the sum of contributions from six polarized valleys.

to interlayer conductivity are from the valley parts, where the Fermi velocities of carriers are parallel to the in-plane fields.[19,20] Such carriers preserve their interlayer velocities and have large current components in the interlayer direction. The interlayer conductivity will take its maximum, and the MR will take its minimum when the field is perpendicular to flat regions of the Fermi surface. The MR peaks are related to the vanishing of the electronic group velocity perpendicular to the layers. Therefore, six inequivalent angular-dependent interlayer MR peaks are expected in the *p*-type Sb_2Te_3, with anisotropic sixfold valley degeneracy and Dirac dispersion (different from the dispersion of surface states) in each valley.

In this multivalley system, in the presence of an in-plane magnetic field, the electric interlayer conductivity is expected to be the sum of the contributions by individual valleys. In the case of Sb_2Te_3,

$$\sigma_{zz} = \sum_{i=1\sim 6} \sigma^i, \tag{1}$$

where the conductivities of hole pockets are indexed by σ^i. Inspired by the fitting for conductivity of Bi in Ref. 18, our experimental data also can be fitted by an empirical formula:

$$\sigma_{zz} = \sum_{i=1\sim 6} \frac{\sigma^i_{\max}}{1+\alpha\cos^2\left[\varphi+(i-1)\frac{2\pi}{6}\right]}. \tag{2}$$

In this configuration, unlike the σ_{bin} in Bi, $\sigma^i_{\max}$ is the maximal σ^i when the field locates at one valley and is different in each valley because the angular-dependent interlayer σ is asymmetrical. The α is a given parameter and represents the anisotropy of interlayer conductivity. Here, $\sigma^i_{\max}$ and α also have temperature and magnetic field dependences.

Sb_2Te_3 has a rhombohedral crystal structure and in the Fermi surface carrier dispersion law is a sum of the in-plane and interlayer terms:

$$\epsilon = \epsilon_{\parallel} + \epsilon_{\perp}, \tag{3}$$

where ϵ is the carrier energy. For the in-plane dispersion law $\epsilon_{\parallel} = \epsilon_{\parallel}(k_x, k_y)$ and for interlayer dispersion law $\epsilon_{\perp} = \epsilon_{\perp}(k_x, k_y, k_z)$.

Here k_x, k_y, and k_z are the electron wave vectors along a, b, and c.

$$\epsilon_{\perp} = -8t_{\perp}\cos k_x\frac{a}{2}\cos\left(k_y\frac{\sqrt{3}}{6}a + k_z d\right) - 4t_{\perp}\cos\left(k_y\frac{\sqrt{3}}{3}a - k_z d\right). \tag{4}$$

Here $a = 4.25$ Å and $d = 2.02$ Å ($c = 30.35$ Å) are the lattice constant and the layer-to-layer spacing of the crystal structure. Within a semiclassical picture, the electron wave vector $\mathbf{k}$ changes in time t according to the Lorentz equation of motion for a hole in a magnetic field:

$$\frac{d\mathbf{k}}{dt} = \frac{e}{\hbar c}(\mathbf{v}\times\mathbf{H}), \tag{5}$$

where $\mathbf{v} = \frac{\partial\epsilon}{\hbar\partial\mathbf{k}}$, e, $\hbar$, c are the hole charge, Planck constant and speed of light, respectively. The interlayer conductivity tensor σ_{zz} can be obtained by solving the linearized Boltzmann equation in the τ approximation:[35]

$$\sigma_{zz} = 2e^2\int\frac{d^3k(0)}{(2\pi)^3}\left(-\frac{\partial f}{\partial\epsilon}\right)\mathrm{v}_z[k(0)]\int_0^{\infty}dt\,\mathrm{v}_z[k(t)]e^{-t/\tau}, \tag{6}$$

$$\mathrm{v}_z[k(0)] = 4t_{\perp}c\left\{2\cos k_x\frac{a}{2}\sin\left[k_y\frac{\sqrt{3}}{6}a + k_z(0)d\right] - \sin\left[k_y\frac{\sqrt{3}}{3}a - k_z(0)d\right]\right\}. \tag{7}$$

When the field B is oriented perpendicular to the current I, the cyclotron motion is approximately parallel to k_z. A strong field localizes all holes except those that have an in-plane velocity that is parallel to B and feels zero Lorentz force. Consequently, taking the integrals of Eq. (7), we find the interlayer conductivity σ_{zz} can be expressed as

$$\sigma_{zz} = \frac{2e^2t_{\perp}^2\tau d}{\pi^2\hbar^3}\int\frac{dk_l}{v}\frac{4\cos^2k_x\frac{a}{2} + 4\cos k_x\frac{a}{2}\cos k_y\frac{\sqrt{3}}{2}a + 1}{1+[\omega_z(\phi)\tau]^2}. \tag{8}$$

Similar equations were also obtained in Refs. 36 and 37.

$$\text{Here, } \omega_z(\phi) = \frac{edH}{\hbar c}(v_x\sin\phi - v_y\cos\phi). \tag{9}$$

$\omega_z(\phi)$ is the cyclotron frequency of hole motion across the Brillouin zone in the k_z direction, where $t_{\perp}$ is the interlayer hopping amplitude, d is the layer-to-layer space, and $l = x, y$. e is the hole charge, which stays constant. In a weak in-plane $\mathbf{B}$, $\omega_z(\phi)\tau \ll 1$, the holes in the valleys represent closed orbits and in a strong in-plane B, $\omega_z(\phi)\tau \gg 1$, holes with open orbits arise. This can be confirmed from the observed high-field, nonsaturated, linear interlayer MR in Fig. 2. However, a small amount of holes with closed orbits also exist in a strong B. Based on the above formula, the angular dependences of interlayer MR on the orientation of B can be understood by considering the cyclotron frequency $\omega_z(\phi)$ and the velocity v_z. Those holes that travel across interlayer with maximal $\omega_z(\phi)$ give rise to minimum σ_{zz} and maximal ρ_{zz}, where the in-plane B is perpendicular to flat regions of the Fermi surface. Therefore, as shown in Fig. 4(b), the steepest valleys in the Fermi surface located at 0° (360°) and 180° with maximal ρ_{zz} appear when B is perpendicular to these regions. In additions, a strong in-plane B localizes all holes except those that feel zero Lorentz force, which have an in-plane velocity parallel to B and contribute to σ_{zz}. So, at 0° (360°) and 180°, the holes that contribute to ρ_{zz} have maximal velocity v and perpendicular to the magnetic fields. On the contrary, when the magnetic fields locate at 60°, 120°, 240°, and 300°, the ρ_{zz} is smaller and these valleys that locate at these positions are more flat. At these degrees, the perpendicular hole velocity v_z and $\omega_z(\phi)$ are also smaller.

In summary, we used the angular dependences of interlayer MR under an in-plane magnetic field to study the field-induced polarization of valleys in the Sb_2Te_3 single crystals. Giant and high-field linear interlayer MR and six unequal peaks were observed in angular-dependent interlayer

MR. The valley polarization is analyzed through resolving a linearized Boltzmann equation in the τ approximation. We hope that this work will stimulate similar experiments and analysis to investigate magnetic field-induced polarization of valleys in other three-dimensional topological insulators such as Bi_2Te_3 and Bi_2Se_3, as well as other multivalley layered compounds.

This work is partially supported by the Australian Research Council through a Discovery project (Grant No. DP1094073).

*Author to whom correspondence should be addressed: xiaolin@uow.edu.au

[1]T. Morinari, H. Nakamura, M. Machida, and T. Tohyama, J. Phys. Soc. Jpn. **78**, 114702 (2009).
[2]W. Kullmann, J. Geurts, W. Richter, N. Lehner, H. Rauh, U. Steigenberger, G. Eichhorn, and R. Geick, Phys. Status Solidi B **125**, 131 (1984).
[3]T. Thonhauser, T. J. Scheidemantel, J. O. Sofo, J. V. Badding, and G. D. Mahan, Phys. Rev. B **68**, 085201 (2003).
[4]Y. Kim, A. DiVenere, G. K. L. Wong, J. B. Ketterson, S. Cho, and J. R. Meyer, J. Appl. Phys. **91**, 715 (2002).
[5]V. A. Kulbachinskii, Z. M. Dashevskii, M. Inoue, M. Sasaki, H. Negishi, W. X. Gao, P. Lostak, J. Horak, and A. de Visser, Phys. Rev. B **52**, 10915 (1995).
[6]V. A. Kulbachinskii, N. Miura, H. Nakagawa, H. Arimoto, T. Ikaida, P. Lostak, and C. Drasar, Phys. Rev. B **59**, 15733 (1999).
[7]V. A. Kulbachinskii, A. Yu Kaminsky, R. A. Lunin, K. Kindo, Y. Narumi, K. Suga, S. Kawasaki, M. Sasaki, N. Miyajima, P. Lostak, and P. Hajek, Semicond. Sci. Technol. **17**, 1133 (2002).
[8]H. Y. Lv, H. J. Liu, L. Pan, Y. W. Wen, X. J. Tan, J. Shi, and X. F. Tang, Appl. Phys. Lett. **96**, 142101 (2010).
[9]G. F. Wang and T. Cagin, Phys. Rev. B **76**, 075201 (2007).
[10]H. J. Zhang, C. X. Liu, X. Liang Qi, X. Dai, Z. Fang, and S. C. Zhang, Nat. Phys. **5**, 438 (2009).
[11]D. Kong, Y. L. Chen, J. J. Cha, Q. F. Zhang, J. G. Analytis, K. J. Lai, Z. K. Liu, S. S. Hong, K. J. Koski, S. K. Mo, Z. Hussain, I. R. Fisher, Z. X. Shen, and Y. Cui, Nat. Nanotechnol. **6**, 705 (2011).
[12]M. Z. Hasan and C. L. Kane, Rev. Mod. Phys. **82**, 3045 (2010).
[13]X. L. Qi and S. C. Zhang, Rev. Mod. Phys. **83**, 1057 (2011).
[14]B. A. Bernevig, T. L. Hughes, and S. C. Zhang, Science **314**, 1757 (2006).
[15]D. Hsieh, D. Qian, L. Wray, Y. Xia, Y. S. Hor, R. J. Cava, and M. Z. Hasan, Nature **452**, 970 (2008).
[16]J. E. Moore, Nature **464**, 194 (2010).
[17]Y. L. Chen, J. G. Analytis, J. H. Chu, Z. K. Liu, S. K. Mo, X. L. Qi, H. J. Zhang, D. H. Lu, X. Dai, Z. Fang, S. C. Zhang, I. R. Fisher, Z. Hussain, and Z. X. Shen, Science **325**, 178 (2009).
[18]Z. W. Zhu, A. Collaudin, B. Fauqué, W. Kang, and K. Behnia, Nat. Phys. **8**, 89 (2012).
[19]N. E. Hussey, J. R. Cooper, J. M. Wheatley, I. R. Fisher, A. Carrington, A. P. Mackenzie, C. T. Lin, and O. Milat, Phys. Rev. Lett. **76**, 122 (1996).
[20]N. E. Hussey, A. P. Mackenzie, J. R. Cooper, Y. Maeno, and S. Nishizaki, and T. Fujita, Phys. Rev. B **57**, 5505 (1998).
[21]R. H. McKenzie and P. Moses, Phys. Rev. Lett. **81**, 4492 (1998).
[22]M. S. Nam, S. J. Blundell, A. Ardavan, J. A. Symington, and J. Singleton, J. Phys.: Condens. Matter **13**, 2271 (2001).
[23]M. Kimata, T. Terashima, N. Kurita, H. Satsukawa, A. Harada, K. Kodama, A. Sato, M. Imai, K. Kihou, C. H. Lee, H. Kito, H. Eisaki, A. Iyo, T. Saito, H. Fukazawa, Y. Kohori, H. Harima, and S. Uji, Phys. Rev. Lett. **105**, 246403 (2010).
[24]X. L. Wang, Y. Du, S. X. Dou, and C. Zhang, Phys. Rev. Lett. **108**, 266806 (2012).
[25]A. A. Abrikosov, Phys. Rev. B **58**, 2788 (1998).
[26]E. Fawcett, Adv. Phys. **13**, 139 (1964).
[27]J. R. Drabble and R. Wolf, Proc. R. Phys. Soc. B (London) **69**, 1101 (1956).
[28]V. A. Kulbachinskii, A. Y. Kaminskii, V. G. Kytin, P. Lostak, C. Drasar, and A. de Visser, JETP **90**, 1081 (2000).
[29]H. Schwartz, G. Björck, and O. Beckmann, Solid State Commun. **5**, 905 (1967).
[30]V. A. Kulbachinski, A. Yu. Kaminski, N. Miyajima, M. Sasaki, H. Negishi, M. Inoue, and H. Kadomatsu, JETP Lett. **70**, 767 (1999).
[31]V. A. Kulbachinskii, M. Inoue, M. Sasaki, H. Negishi, W. X. Gao, K. Takase, Y. Giman, P. Lostak, and J. Horak, Phys. Rev. B **50**, 16921 (1994).
[32]D. A. Abanin, S. A. Parameswaran, S. A. Kivelson, S. L. Sondhi, Phys. Rev. B **82**, 035428 (2010).
[33]E. Fradkin, S. A. Kivelson, M. J. Lawler, J. P. Eisenstein, and A. P. Mackenzie, Annu. Rev. Condens. Matter Phys. **1**, 153 (2010).
[34]L. Li, J. G. Checkelsky, Y. S. Hor, C. Uher, A. F. Hebard, R. J. Cava, and N. P. Ong, Science **321**, 547 (2008).
[35]A. Dragulescu, V. M. Yakovenko, and D. J. Singh, Phys. Rev. B **60**, 6312 (1999).
[36]A. G. Lebed and N. N. Bagmet, Phys. Rev. B **55**, R8654 (1997).
[37]A. J. Schofield and J. R. Cooper, Phys. Rev. B **62**, 10779 (2000).